Chaos, Solitons and Fractals 186 (2024) 115199

Contents lists available at ScienceDirect

Chaos, Solitons and Fractals

journal homepage: www.elsevier.com/locate/chaos

Understanding post-angiogenic tumor growth: Insights from vascular network properties in cellular automata modeling

Juan Uriel Legaria-Peña, Félix Sánchez-Morales, Yuriria Cortés-Poza *

IIMAS, Unidad Académica de Yucatán, Universidad Nacional Autónoma de México (UNAM), Yuc., Mexico

ARTICLE INFO

Keywords:
Angiogenesis modeling
Complex systems
Network analysis
Cellular automata
VDA therapy

ABSTRACT

Angiogenesis plays a crucial role in tumor progression and is a key target for cancer therapy. This study utilizes a novel cellular automata model to explore post-angiogenic tumor growth, focusing on vascular network properties. We simulate the effects of Vascular Disrupting Agents (VDA) and radiotherapy, analyzing how network parameters, such as clustering coefficient and degree distribution, influence tumor progression and treatment outcomes.

Our model reveals that highly clustered vascular networks with low average path lengths are more resistant to VDA therapy and radiotherapy, whereas more homogeneous networks are more susceptible. Disruptions in network integrity significantly impair nutrient delivery, leading to heterogeneous tumor growth patterns. Quantitative analyses show strong correlations between network metrics and treatment response, suggesting that targeted modulation of vascular network properties could enhance therapeutic effectiveness. These findings offer new insights into tumor-vascular interactions and propose potential avenues for optimizing cancer treatment protocols.

1. Introduction

Cancer remains an elusive threat to human health, even when research on the pathology has substantially increased compared to other diseases [1]. As we delve into understanding the mechanisms of cancer, more questions are brought to light, and new lines of research are opened. In part, this can be attributed to the complex nature of the disease, which allows it to exhibit a wide range of presentations, identifiable growth stages, and adaptive strategies [2].

In tackling the complexity of cancer, developing multidisciplinary approaches at the confluence of medicine, molecular biology, physics, and computer science are deemed essential. These can help unravel how patterns of organization and adaptation emerge in cancer from interactions among malignant cells and between these cells and their environment [3].

One of the points in cancer development where a tumor can exhibit notoriously complex and invasive traits is during its vascular phase. In such a stage, the proliferating cancer cells are supplied with nutrients and oxygen by a vascular network formed around the tumor through a process known as angiogenesis [4].

Complex approaches that use networks to analyze vascular structures in the tumor's environment have been proposed in some studies. In [5], Anahita Fouladzadeh et al. used cell live imaging to study how some network properties evolved in time as vascular networks were formed in-vitro, concluding that endothelial cells can increase the clustering coefficient of blood-vessel networks. In [6], Juan Carlos Chimal-Eguía et al. extracted vascular network properties from tomographic images, characterizing their clustering coefficient and the shape of their degree distribution. Pawel Topa and Witold Dzwinel proposed using global network descriptors such as graph density and total degree to characterize and classify tumor vascular networks [7]. Bernadette J. Stolz et al. studied the topological qualities of 3D vascular networks collected using intravital and ultramicroscopy in [8]. Namely, they investigated how network tortuosity and loops change in response to antibodies and the effect of radiotherapy.

Besides networks, other complex systems modeling strategies have been applied to simulate how blood vessel branches develop during angiogenesis from the interaction of local biomolecules. In this regard, we highlight Cell-based methods, specifically Cellular Automata (CA). CA models allow us to compute how blood vessels propagate in a lattice and have been used to investigate different aspects of vascular formation, such as perfusion of chemotherapy drugs in a vascular tumor-induced network [9], fractal characteristics of growing capillary sprouts [10]. The effects of administering anti-angiogenic components, such as angiostatin [11].

Several models have been proposed to explore vascular tumor growth. One of the most essential features of these models is the

* Corresponding author.
E-mail address: yuriria.cortes@iimas.unam.mx (Y. Cortés-Poza).

https://doi.org/10.1016/j.chaos.2024.115199
Received 20 March 2024; Received in revised form 11 June 2024; Accepted 20 June 2024
Available online 1 July 2024

capacity to simulate tumor growth as tumor cells absorb oxygen from the existing vasculature. Shirinifard et al. presented a 3D simulation in [12]. Their model is allowed to grow to a maximum diameter before the dynamics of the vascular phase are activated. During this phase, the tumor grows as new vasculature is formed synchronized. Models like these, including ours, provide a platform for examining how angiogenesis can affect the proliferation rate of cancer cells.

In this work, we study how different vascular network properties are related to tumor growth and treatment outcomes in a proposed cellular automata model for angiogenic cancer development. The model simulates tumor growth and angiogenesis in an interactive synchronous fashion. Such a model is proposed as an extension of a CA for tumor growth and therapy introduced in [13]. Our experiments simulate a blood vessel network formation around a developing avascular tumor. Then, we make a point measurement of the network to extract four global features of interest: (1) average degree centrality, (2) average betweenness centrality, (3) average page rank, and (4) average clustering coefficient. After this characterization, we let the system develop further and assess tumor growth through Shannon's entropy, which has been identified as a sensitive biomarker for cell dissemination in our CA. Such a procedure allows us to study how vascular network characteristics influence tumor proliferation. Furthermore, we assess how these properties are related to tumor response for two distinct treatments: radiotherapy and a novel model for vascular disrupting agents (VDA) that we introduce in this work. Our VDA therapy allows us to explore how attacking specific network sections affects tumor propagation.

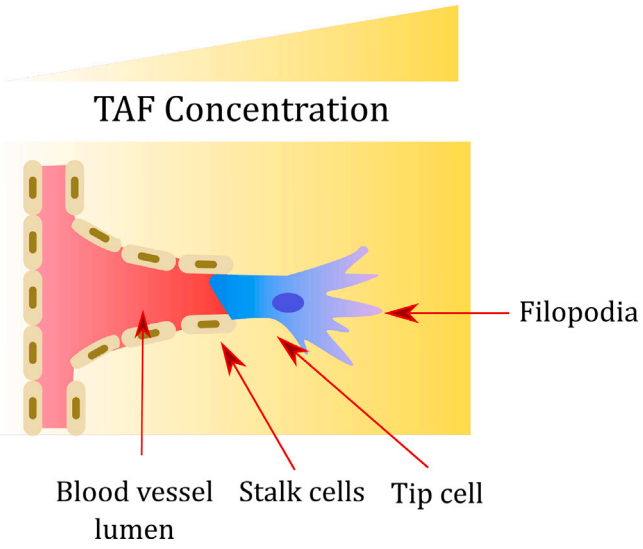

Fig. 1. Illustration of sprout angiogenesis. Tip cells lead the branch towards regions of high TAF concentration, providing the environment using Filopodia. On the other hand, stalk cells trail behind to form the lining separating the blood vessel lumen from the exterior. Regions of high accumulation of angiogenic factors are marked in the scheme with an opaque yellow color. (For interpretation of the references to color in this figure legend, the reader is referred to the web version of this article.)

2. Background

2.1. Angiogenesis in cancer

Angiogenesis, the new blood vessel formation process, plays a pivotal role in tumor progression by supplying oxygen and nutrients to proliferating cancer cells. It is involved in distinct physiological processes and diseases, such as embryogenesis, wound healing, arthritis, and most relevant to this work, in cancer development [14]. In the context of cancer, sprouting angiogenesis is a crucial mechanism where tumors stimulate nearby blood vessels to sprout and form capillaries that infiltrate the tumor mass. This process is initiated when a tumor reaches a size limit where diffusion alone cannot sustain its growth, prompting cancer cells' secretion of tumor angiogenesis factors (TAFs). Sprouting angiogenesis facilitates establishing a vascular network around the tumor and promotes metastatic dissemination [15] by providing cancer cells with access to the circulatory system.

The primary mechanism by which a network of blood vessels is formed around a tumor is sprouting angiogenesis, where blood vessels are formed from pre-existing ones, creating capillary branches that reach the tumor. In sprouting angiogenesis, endothelial cells are guided by specific signaling molecules, most notably vascular endothelial growth factors (VEGFs) [16]. These propagating endothelial cells eventually form an inner lining tissue that coats blood vessels, separating their lumen from the exterior. They also signal and organize the formation of outer layers with connective tissue to ensemble the external wall of blood vessels [17].

The movement of endothelial cells during sprouting angiogenesis requires the coordination of two distinct phenotypes: tip cells and stalk cells. Tip cells, characterized by their high motility, lead the development of sprouts. They possess specialized fibrillary structures called filopodia in their membrane, enabling interactions with the environment that influence cell adhesion and detachment [18]. In contrast, stalk cells trail behind tip cells and are responsible for consolidating the formation of blood vessel lumens (inside space of vessels) and extending developing sprouts [19].

In Fig. 1, we depict sprouting angiogenesis. It can be observed that the tip cell leads the movement of the branch toward regions where TAFs are highly concentrated, while stalk cells stay behind, consolidating the formation of blood vessels.

In addition to pro-angiogenic factors, various components influence the development of vascular networks. One such component that will be considered in the methods of this study is fibronectin. Fibronectin forms a family of glycoproteins that can self-organize into arrays, facilitating cell mobility within the extracellular matrix [20]. Endothelial cells possess integrins that recognize fibronectin, aiding their adhesion and enabling faster advancement through the extracellular matrix to nourish the tumor [21]. Furthermore, endothelial cells can synthesize fibronectin, presenting a mechanism through which they shape their environment to optimize navigation [22].

2.2. Role of angiogenesis in cancer treatment

Angiogenesis plays a critical role in cancer treatment, as it facilitates the rapid spread of malignant cells, presenting significant challenges for therapy. This challenge is exacerbated by the dynamic nature of cancer growth and its adaptive mechanisms, particularly during the vascular phases of the disease [23]. One factor influencing treatment efficacy is the morphology of the nutrient-supplying network. Studies have shown that the effects of radiotherapy are more pronounced in regions of the tumor where the configuration of blood vessels is sparse, leading to conditions of local hypoxia [24,25].

Given the importance of blood vessel supply in cancer progression, various therapies have been proposed to target vascular networks. These treatments aim to prevent vascular network formation or disrupt existing blood vessels. Anti-angiogenic therapy, for example, inhibits signaling pathways for vascular endothelial growth factors (VEGFs), thereby halting the creation of new blood vessels [26]. Conversely, vascular disrupting agents (VDAs) target established blood vessels in the tumor environment, leading to their elimination [27]. In this study, we propose and assess a model for VDA treatment, detailed in 3.4.

2.3. Cellular automata and complex networks

Cellular Automata (CA) and Complex Networks are mathematical and computational models commonly used to explore complex systems.

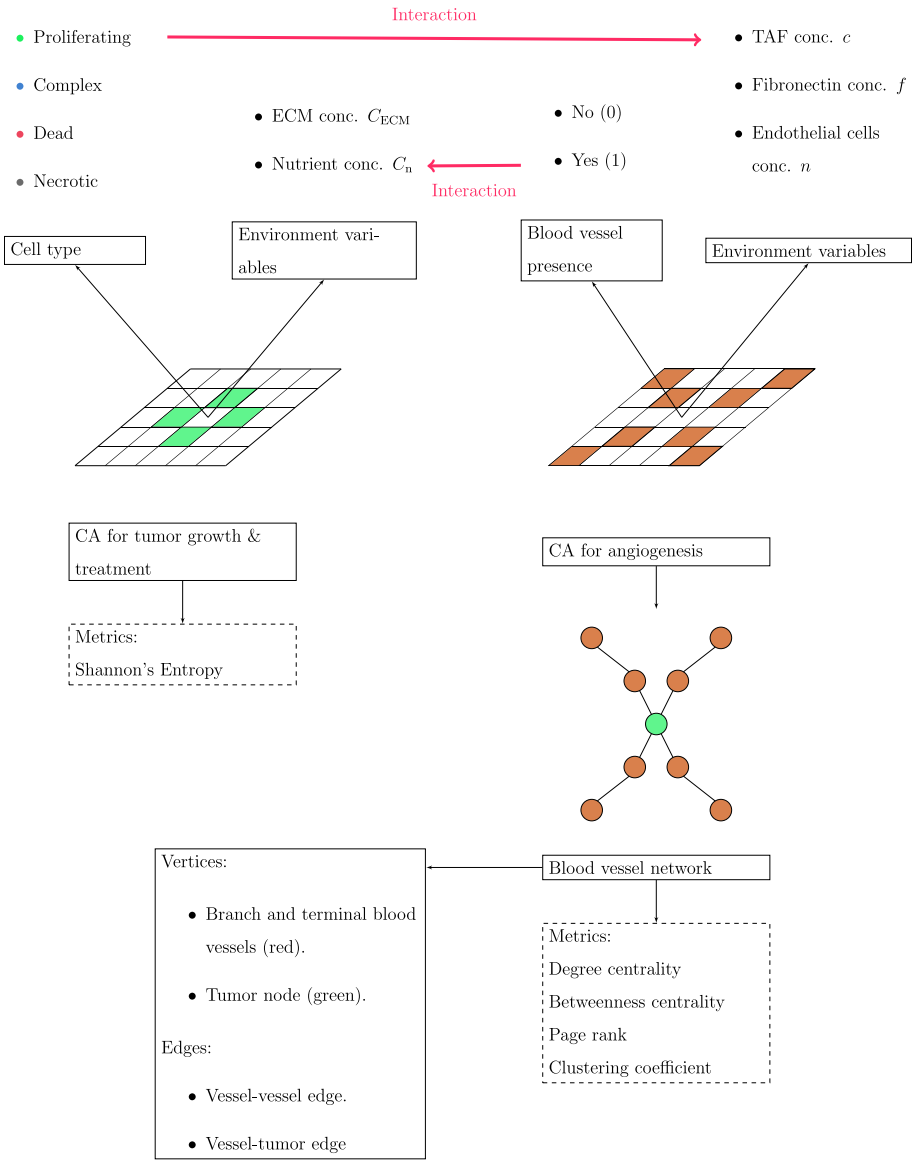

Fig. 2. Scheme of the state variables used in the two cellular automata models applied in this work to simulate tumor growth and angiogenesis. In the case of the tumor growth automata, Shannon's entropy was used as a biomarker for cancer development and therapy outcomes. The blood vessel grid generated by the angiogenesis CA can be transformed into a network to assess graph properties at any simulation point. This analysis allowed us to explore the relationship between such network features and vascular tumor growth and therapy prognosis. The automata's interaction points are two-fold: blood-vessel presence provides nutrients for the tumor, and proliferating cell presence increases the tumor angiogenic factor (TAF) concentration. (For interpretation of the references to color in this figure legend, the reader is referred to the web version of this article.)

These models help portray the interrelationships among system components and compute the dynamics and organized patterns that emerge from their interactions.

In CAs, the components of the system occupy cells in a lattice, with their state being described by a discrete number of variables. At every step of the automaton's evolution, a new state is computed for all cells, where the next state of a given cell will be a function of its current state and that of its neighboring cells. When such computation is carried out iteratively, it is possible to observe how repeated local interactions result in collectively organized patterns.

This work merges two cellular automata models to simulate tumor growth in the vascular phase. The first model's tumor growth and treatment, while the second simulates blood vessel formation around dynamically proliferating cancer cells. Both automata interact with each other and can be evolved concurrently.

Fig. 2 summarizes the properties of CA and network models used in this work and the metrics used to assess each. In the CA for tumor growth, each space can be occupied by four biological cell variants: proliferating, complex, dead, and necrotic. In addition, two environmental variables influence changes in the state of a cell: the concentrations of nutrients and ECM. In the vascular phase, nutrient concentration is determined by the locations occupied by blood vessels in the angiogenesis automaton, which is one of the interaction points between them. Rules applied to update the state of a cell in the tumor growth CA will be established in detail in Section 2.4. In the case of the angiogenesis CA, a lattice is considered, which indicates the presence/absence of blood vessels (0: No, 1: Yes). Changes in this state variable are influenced by three environmental variables: concentrations for TAF, fibronectin, and endothelial cells. TAF depends on the location of cancer proliferating cells, providing the second point of overlap between the automata. Rules applied to evolve the angiogenesis model will be explained in Section 3.1.

Regarding assessment metrics, the model relies on Shannon's entropy as a tumor growth and treatment biomarker. Previous studies

showed that this quantity increased with tumor growth and decreased when simulated therapy was administered.

If T_i denotes the ith biological cell type considered in the model, where T_i can be either proliferating, complex, or dead, *Shannon's entropy* for the CA can be computed using the following equation:

$$S = \sum_{i=0}^{N} P(T_i) \log\left(\frac{1}{P(T_i)}\right) \tag{1}$$

where $P(T_i)$ is the probability of observing the ith cell type. Such probability can be obtained by adding the number of cells of type T_i across the automaton and dividing the count by the total number of occupied automaton cells.

Networks or graphs are structures where vertices denote the components of a system, while edges represent links or relations between them. In this work, a network can be constructed from the angiogenesis automaton at any point in the simulation. As indicated in Fig. 2, nodes in such a network denote branching or terminal points in the blood vessel array. On the other hand, edges indicate whether nodes are close to each other and in the same branch. In addition, we use a node representing the tumor (green node in the figure). The nodes connected to it are those spatially close to proliferating cells when the lattices of both automata are superposed. Conversion of the blood vessel array into a graph allowed us to examine how distinct network metrics were related to tumor growth and treatment prognosis. The metrics under investigation in this study were degree centrality, betweenness centrality, page rank, and clustering coefficient. The definition for such quantities is the following:

- *Degree centrality*:
  Degree centrality is a measure of how connected a given vertex is. Denoting the number of edges associated with vertex v as $d(v)$, and assuming the total number of vertices in the network is N_V, degree centrality of v can be computed using the following equation:

$$C_D(v) = \frac{d(v)}{N_V - 1} \tag{2}$$

- *Betweenness centrality*: *Betweenness centrality* is a metric that measures the amount of shortest paths in a graph that passes through a given node v. If $\sigma(s,t)$ denotes the number of shortest paths between two arbitrary distinct vertices s,t, and $\sigma_v(s,t)$ is the number of those paths that cross through v, betweenness centrality can be obtained as shown in Eq. (3).

$$C_B(v) = \sum_{s,t \in V | s \neq t \neq v} \frac{\sigma_v(s,t)}{\sigma(s,t)} \tag{3}$$

  where the sum runs over all pairs of vertices in the graph.
- *Page rank*:
  Page rank is an algorithm created by Google to rank websites. The central idea is that the most ranked nodes are the ones that can be reached through many other high-ranked vertices. To calculate the page rank of a node v, we first consider a constant dampening parameter γ_d, which is usually assigned a value of 0.85. Then, if $k(w)$ denotes the number of outward edges associated with a vertex $w \neq v$ which is connected to v ((w,v) belongs to the set of edges E), a new page rank value for v can be obtained as follows:

$$PR(v) = (1 - \gamma_d) + \gamma_d \sum_{(w,v) \in E | w \neq v} \frac{PR(w)}{k(w)} \tag{4}$$

  In practice, this equation is iteratively applied to every vertex until the change in page rank for every node is less than a given threshold.
- *Clustering coefficient*:
  Finally, the clustering coefficient measures the extent to which nodes cluster around a given vertex v. If we denote the set that contains v and other nodes connected to v as $\mathcal{N}_v$, and N_v is the number of edges in the graph between any pair of elements in the set $\mathcal{N}_v$, the clustering coefficient of v in an undirected graph can be obtained in the following way:

$$C_C(v) = \frac{2N_v}{|\mathcal{N}_v|(|\mathcal{N}_v| - 1)} \tag{5}$$

  where $|\mathcal{N}_v|$ is the cardinality (number of elements) of the set $\mathcal{N}_v$.

2.4. Tumor growth CA

In this work, we extended a previous CA model we proposed for avascular tumor growth and therapy in [13] to explore cancer behavior in the vascular phase.

A first glimpse of the components contemplated in the automaton is shown in Fig. 2. As mentioned, different types of biological cells can occupy spaces in the automaton's grid. The rules for updating cell type and environment variables (concentrations of nutrient and ECM) are described in Table 1.[1] In the case of nutrients, the rule depends on the state of the angiogenesis automaton. Specifically, suppose the position to update is occupied by a blood vessel. In that case, the nutrient concentration is assigned a constant value C_{BV} (the constant nutrient concentration produced by the blood vessel at each step); otherwise, we apply a diffusion rule with a dissipation term to compute the new nutrient value.

In Table 1 the parameter D_{nut} is the diffusion coefficient of the nutrient. In the second Fick's used law, this quantity describes how fast nutrient diffuses over the automaton's area due to existing local concentration gradients. On the other hand, C_{abs} represents the constant amount of nutrient concentration that cells absorb at each step of the simulation. Regarding ECM concentration, the law used for updating describes the degradation of ECM due to tumor growth. Such degradation is proportional to $I(i,j)$: the number of proliferating cells surrounding the lattice space (i,j), and the proportionality constant is given as e_c. This rule was originally posed based on the model presented by Shahmoradi et al. in [29].

2.5. Radiotherapy model

The radiotherapy model is based on Sarah C. Brüningk et al.'s presentation in [30]. Namely, we apply an adaptation of the Linear–quadratic response function (LQ), an empirical law that describes the effects of radiation on biological tissue. This law has been experimentally validated in animal studies and is sometimes applied in clinical settings for distributing the radiation dose over multiple sessions (dose fractionation) [31,32].

The response function of radiotherapy indicates the probability P_{rad} that a cell is targeted by radiotherapy at position (i,j) of the automaton. The LQ equation that describes such a response is the following:

$$P_{\text{rad}}(i,j) = 1 - \exp\left(-\gamma_{\text{rad}}\left(\alpha_{\text{rad}} d_{\text{OER}}(i,j) + \beta_{\text{rad}} d^2_{\text{OER}}(i,j)\right)\right) \tag{6}$$

here α_{rad} and β_{rad} are fixed parameters.

The factor γ_{rad} appearing in the previous equation considers that radiotherapy acts more effectively at certain stages of the cell's reproduction cycle. Its calculation is conducted as indicated by Eq. (7).

$$\gamma_{\text{rad}} = \gamma_{0,\text{rad}} \times 1.5^{(n - s_0)\%4} \tag{7}$$

Here, $\gamma_{0,\text{rad}}$ is a constant, s_0 is the simulation step at which the cell first spawned, and n denotes the current iteration of the CA evolution. The symbol % denotes a modulus operation.

[1] Lefever and Erneaux analyzed the parameters r_{prolif}, r_{binding}, r_{lysis} and r_{decay} for their sensitivity, highlighting how even subtle modifications can result in varied adaptive responses [28].

Table 1
Update rules of the CA for tumor growth. In the rule for ECM concentration update, e_c denotes a constant parameter, while $I(i,j)$ is the number of neighbors to location (i,j) surrounded by proliferating cells. On the other hand, in the expression used to update nutrient concentration, D_{nut} and C_{abs} are constant parameters. C_{BV} denotes the constant nutrient concentration assigned to positions where blood vessels are present.

Cell type transition rules	
• Proliferating	• Place a new proliferating cell at neighboring position with probability r_{prolif} if concentration of ECM at the location is low. 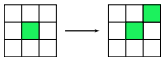
	• If the nutrient concentration is low, transition to necrotic. 
• Complex	• Turn to complex with probability $1 - r_{\text{binding}}$ (cell is neutralized by the immune system). 
	• Return to proliferating with probability r_{escape} (cell escapes the immune system). 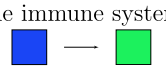
	• Transition to dead with probability r_{lysis} (cell is eliminated by the immune system). 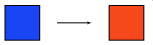
• Dead	• Dead cells turn to healthy tissue (vacant automaton cells) with probability r_{decay}. 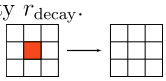
ECM Concentration update	
$C^{\text{new}}_{\text{ECM}}(i,j) = C_{\text{ECM}}(i,j) - e_c I(i,j) C_{\text{ECM}}(i,j)$	
Nutrient concentration update	
If blood vessel at (i,j)	$C^{\text{new}}_n(i,j) = C_{BV}$
Otherwise	$C^{\text{new}}_n(i,j) = C_n(i,j) + D_{nut}\nabla^2 C_n(i,j) - C_{\text{abs}}$

Finally, the term d_{OER} in Eq. (6) is named the oxygen status of the cell. This quantity depends on the nutrient concentration C_n at the location in question and the radiation dosage d applied to the in-silico tissue. Its calculation requires the application of Eqs. (8) and (9).

$$d_{OER} = \frac{d}{\text{OER}} \tag{8}$$

$$\text{OER} = \begin{cases} 1 & C_n(i,j) \geq T_{n,\text{rad}} \\ 3 - \frac{2C_n(i,j)}{T_{n,\text{rad}}} & C_n(i,j) < T_{n,\text{rad}} \end{cases} \tag{9}$$

where $T_{n,\text{rad}}$ is a fixed threshold.

Once the cells to be targeted are chosen based on the radiotherapy response function, they can undergo cell death whenever they are proliferating. Cell death by radiotherapy can be necrotic with probability R_{nec}, or the cell could turn to a death state with probability $1 - R_{\text{nec}}$. The probability of death in post-therapy steps occurs with probability $P_{0,\text{rad}}$ for an initial number of steps (50 in the conducted tests) and then with a final probability $P_{f,\text{rad}}$. This simulates the delayed onset of acute radiotherapy effects, frequently observed when irradiating biological tissue [33].

3. Proposed model

Methods applied in this work to study how vasculature network properties affect tumor growth and treatment are presented in this section Parameters in Section 3.1 mainly were adjusted according to the values provided by Alexander R.A. Anderson and Mark A.J. Chaplain in [34]. The authors describe how the applied values arise from existing experimental data in such work. We selected a different set of values for the η parameter, appearing in Eq. (16). In this case, the values were chosen so that the centrality degree of the resulting capillary network could be varied, allowing us to assess the effect of graph properties on tumor growth. In the case of the proposed treatment, VDA (section 3.4), we manually set the parameters to values where an effect on tumor growth could be observed so that we could analyze how targeting specific nodes of the vascular network affects tumor development. Parameter sensitivities are inherited from the source models, and we recommend applying similar values when extending the model or performing similar analysis..

A Python 3 implementation of the models and tests has been available for consultation at [35].

3.1. Cellular automata model for angiogenesis

The proposed cellular automaton for angiogenesis was based on a benchmark model presented by Anderson and Chaplain in [34]. In this case, their methods were adapted to simulate vascular growth around a developing tumor, simulated with the model introduced in Section 2.4. Merging both models involved establishing distinct interactions, which are: (1) nutrient boundary conditions for the tumor change in dynamic fashion as the blood vessel network grows, (2) Concentration of tumor angiogenic factors depends on the locations of proliferating cancer cells, and (3) Addition of tip-cells through branching is more likely at locations close to the tumor (where concentration of TAF is high).

In our simulations, we first evolve an avascular tumor and adjust the concentration of TAF based on cancer cell locations. Then, we incorporate the angiogenesis module, allowing the tumor and blood vessel structure to develop together. At a midway point in time, we then characterize the properties of the vascular network. Finally, we let the tumor and vasculature develop further to establish how the network properties relate to tumor growth and therapy.

The angiogenesis model considers a set $\mathcal{T}$ of sprout tip cells, which can propagate across the automaton's rectangular grid. As tip cells move, they leave a trail of blood vessels, marking their visited positions on a matrix b, which represents an image of the evolved capillary network. Initially, a number T of sprout tips are placed in the boundaries of the automaton, separating them by a fixed number of lattice spaces. Then, at all steps, each tip can move to one of the cells in its 4-neighborhood or stay at its current location based on probabilities that depend on the biochemical environment at the position (i, j) where the tip cell is located. Specifically, the variables that determine the biochemical environment at every location of the automaton are endothelial cell concentration $n(i, j)$, fibronectin concentration $f(i, j)$, and angiogenic factor concentration $c(i, j)$, where initialization and update of c depend on the locations occupied by proliferating cells in the tumor growth automata. Adding new sprout tips to the set $\mathcal{T}$ can occur when old tips branch out, as will be detailed later in this section. Deletion of sprout tips, on the other hand, will take place whenever two different tips collide at the exact location of the grid. In this situation, the two of them will merge, simulating a process known as anastomosis. In terms of the model, one will be removed from $\mathcal{T}$, while the remaining one will be left to evolve. The algorithm used to update the angiogenesis automaton at each step has been summarized in Fig. 3.

We will next describe the rules used to initialize and update the concentrations of endothelial cells n, fibronectin f, and tumor angiogenesis factors c at every location of the automaton as we will see, an algebraic treatment of the rule used to update n leads to a formulation of the probabilities of sprout tip movement in every direction.

To initialize values for n, c, and f, we use a matrix p containing a value of one at locations occupied by proliferating cancer cells in a previously evolved avascular tumor. Denoting the set containing locations (i', j') where $p(i', j') = 1$ as $\mathcal{P}$, we can establish initial conditions for the angiogenesis model using Eqs. (10)–(12).

$$c_0(i,j) = \begin{cases} 2 + \sum_{(i',j')\in\mathcal{P}} \frac{(\nu - \|(i',j')-(i,j)\|)^2}{(\nu-0.1)} & (i,j) \in \mathcal{P} \\ \sum_{(i',j')\in\mathcal{P}} \frac{(\nu - \|(i',j')-(i,j)\|)^2}{(\nu-0.1)} & \text{otherwise} \end{cases} \tag{10}$$

$$f_0(i,j) = 1 \qquad \forall (i,j) \tag{11}$$

$$n_0(i,j) = 0 \qquad \forall (i,j) \tag{12}$$

The form of Eq. (10) arises from computing a steady-state solution for TAF concentration, considering that the tumor is approximately circular [36]. In such expression ν is a fixed parameter and $\|(i', j') - (i, j)\|$ denotes the euclidean distance between locations (i', j') and (i, j). The calculation assigns higher concentration values to positions occupied by cancer cells, and such concentration diminishes for points farther away from the tumor. In practice, the values of $c_0(i, j)$ were normalized by dividing them with the maximum concentration observed across all automaton cells. After this initialization, angiogenesis and tumor growth will occur together, and $c(i, j)$ will be reinforced at locations invaded by cancer cells. Such a rule will be detailed later in this section.

The evolution of endothelial cell concentration is driven by three main processes: (1) diffusion (random movement), (2) chemotaxis, which follows the gradient of tumor angiogenic factors ∇c, and (3) haptotaxis, guided by the gradient of fibronectin concentration ∇f. Based on these mechanisms, its update rule is given as follows:

$$\begin{aligned} n(i,j)^{\text{new}} =& n(i,j) + D_n \nabla^2 n(i,j) - \nabla \cdot (\chi(c(i,j)) n(i,j) \nabla c(i,j)) \\ & - \nabla \cdot (\rho_0 n(i,j) \nabla f(i,j)) \end{aligned} \tag{13}$$

the three successive terms appearing in the expression correspond to diffusion, chemotaxis, and haptotaxis. In this equation, D_n is a diffusion coefficient, ρ_0 is a hypotactic coefficient, and $\chi(c)$ is a chemotactic function, which in this case follows a receptor kinetic law of the form:

$$\chi(c(i,j)) = \frac{\chi_0}{1 + \alpha c(i,j)} \tag{14}$$

The previous Equation reflects that the receptor sensitivity of tip-cells decreases with higher TAF concentrations. χ_0, the chemotactic coefficient, and α are positive parameters of kinetic model.

Something important to note is that operators appearing in the update rules given in this section are applied in their discrete form, which uses finite differences.

The concentration of fibronectin can change in the model in two ways: (1) by synthesis of fibronectin by endothelial cells and (2) through degradation, which might occur when endothelial cells come into contact with the extracellular matrix. Considering this process, the rule used to update fibronectin concentration at location (i, j) of the automaton is stated in Eq. (15).

$$f(i,j)^{\text{new}} = f(i,j) + k\beta n(i,j) - k\gamma n(i,j) f(i,j) \tag{15}$$

where k is a scaling factor, parameter β determines the production of fibronectin by endothelial cells, and γ modulates the uptake of such proteins.

Finally, changes in TAF concentration depend on proliferating cell locations. Namely, we apply a capped increment C_{inc} in concentration if there is a cancer cell and use a diffusion/dissipation rule otherwise (Eq. (16)). Furthermore, we apply a dissipation to all cells, more significantly at regions near the tumor (Eq. (17)), since already innervated sections do not produce further angiogenic factor signaling.

$$c(i,j)^{new} = \begin{cases} c(i,j) + C_{\text{inc}} & c(i,j) < C_{\max} \quad \text{and} \quad p(i,j) = 1 \\ c(i,j) + D_c \nabla c - C_c & \text{otherwise} \end{cases} \tag{16}$$

$$c(i,j)^{new} = c(i,j) - k\eta n(i,j) c(i,j) \tag{17}$$

In such a rule, the parameter η measures the uptake of TAF by endothelial cells, D_c is the diffusion coefficient for angiogenic factors, C_c represents the constant metabolic degradation of such factors, $C_{\max}$ is the maximum allowed value for TAF concentration allowed in the automaton, and C_{inc} is a fixed increment for TAF concentration, which is applied at positions occupied by proliferating cells.

Since sprout tips are a phenotype of endothelial cells, their movement tends to mirror spatial changes in endothelial cell concentration n. Thus, to find probabilities of sprout tip movement in every direction, we can start from Eq. (13) and group terms that refer to values of n in the same direction (left, right, up, down, and center) relative to a central position (i, j) in the automaton's grid. Such treatment leads to the following equation:

$$\begin{aligned} n(i,j)^{\text{next}} =& n(i,j) + P_{\text{center}} n(i,j) + P_{\text{left}} n(i,j-1) + P_{\text{right}} n(i,j+1) \\ & + P_{\text{up}} n(i-1,j) + P_{\text{down}} n(i+1,j), \end{aligned} \tag{18}$$

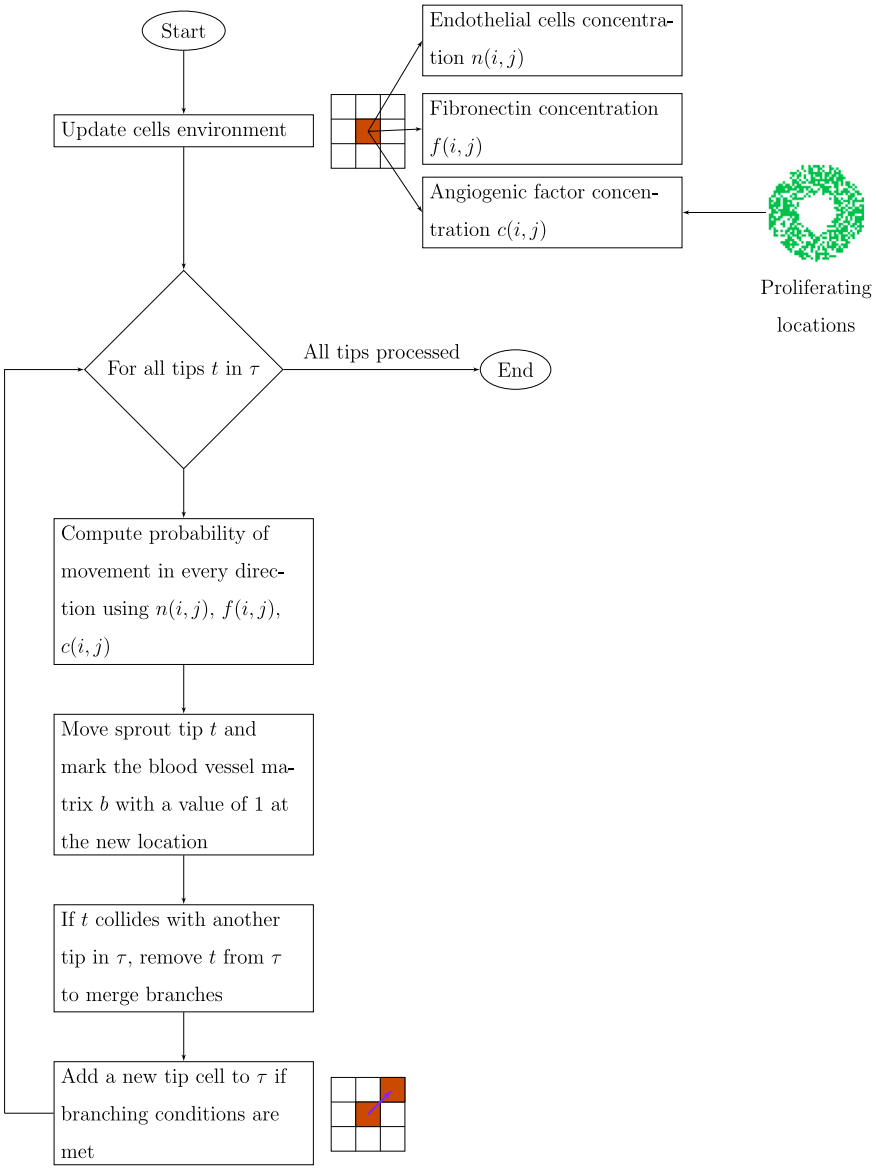

Fig. 3. Algorithm used to update the angiogenesis automaton at each simulation step.

where:

$$\begin{aligned} P_{\text{center}} = 1 &- \frac{kD_n}{h^2} \\ &+ \frac{k\alpha\chi(c(i,j))}{4h^2(1+\alpha c(i,j))}\left((c(i,j+1)-c(i,j-1))^2\right. \\ &+ \left.(c(i-1,j)-(i+1,j))^2\right) \\ &- \frac{k\chi(c(i,j))}{h^2}(c(i+1,j)+c(i-1,j)+c(i,j-1) \\ &+ c(i,j+1)-4c(i,j)) \\ &- \frac{k\rho}{h^2}(f(i+1,j)+f(i-1,j)-4f(i,j)+f(i,j+1)+f(i,j-1)) \end{aligned} \tag{19}$$

$$\begin{aligned} P_{\text{left}} = \frac{kD_n}{h^2} &- \frac{k\chi(c(i,j))}{4h^2}(c(i,j+1)-c(i,j-1)) \\ &+ \frac{k\rho_0}{h^2}(f(i,j+1)-f(i,j-1)) \end{aligned} \tag{20}$$

$$\begin{aligned} P_{\text{right}} = \frac{kD_n}{h^2} &+ \frac{k\chi(c(i,j))}{4h^2}(c(i,j+1)-c(i,j-1)) \\ &+ \frac{k\rho_0}{h^2}(f(i,j+1)-f(i,j-1)) \end{aligned} \tag{21}$$

$$\begin{aligned} P_{\text{up}} = \frac{kD_n}{h^2} &+ \frac{k\chi(c(i,j))}{4h^2}(c(i-1,j)-c(i+1,j)) \\ &+ \frac{k\rho_0}{h^2}(f(i-1,j)-f(i+1,j)) \end{aligned} \tag{22}$$

$$\begin{aligned} P_{\text{down}} = \frac{kD_n}{h^2} &- \frac{k\chi(c(i,j))}{4h^2}(c(i-1,j)-c(i+1,j)) \\ &+ \frac{k\rho_0}{h^2}(f(i-1,j)-f(i+1,j)) \end{aligned} \tag{23}$$

In Eqs. (19)–(23), h represents the physical distance between adjacent cells in the automaton's grid. Values for P obtained in this way are used as probabilities of sprout tip movement in every possible direction. One detail to note is that such quantities might not sum up to 1 in practice, which is required to interpret them as probabilities. For this reason, in our implementation, we first apply the following normalization rule:

$$P_{\text{dir,norm}} = \frac{P_{\text{dir}} - m_P}{\sum_{dir}(P_{\text{dir}} - m_P)} \tag{24}$$

where m_P is the minimum value of P obtained over all the 5 directions considered.

One aspect that remains to be established is the conditions required for the branching of sprout tips. Three criteria have to be satisfied for

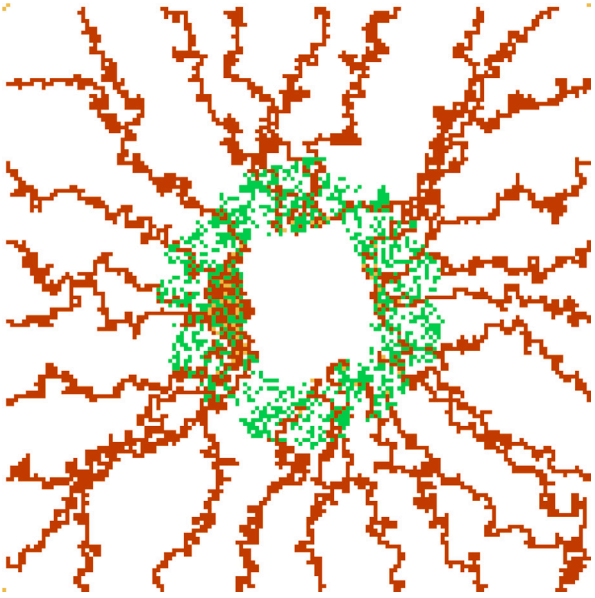

Fig. 4. Example of blood vessel structure formed around a tumor, simulated for 150 steps using the angiogenesis cellular automata. The values used for parameters contemplated in the angiogenesis model were: $n_{\text{steps}} = 150$, $D_n = 0.00035$, $\rho_0 = 0.34$, $\chi_0 = 0.38$, $\alpha = 0.6$, $\beta = 0.05$, $k = 0.0725$, $\gamma = 0.1$, $\eta = 0.035$, $h = 0.005$, $T_{\text{branch}} = 2$, $k_{\text{branch}} = 0.75$, $C_{\text{inc}} = 0.01$, $C_{\text{max}} = 20$, $C_c = 0.001$, $D_c = 0.01$. On the other hand, tumor growth parameter values used were: $r_{\text{prolif}} = 0.8$, $r_{\text{binding}} = 0.3$, $r_{\text{escape}} = 0.5$, $r_{\text{lysis}} = 0.35$, $r_{\text{decay}} = 0.35$, $e_c = 0.1$, $D_{\text{nut}} = 0.01$, $C_{\text{abs}} = 0.01$, $C_{BV} = 2$. (For interpretation of the references to color in this figure legend, the reader is referred to the web version of this article.)

a tip at position (i, j) to be able to branch: (1) that the number of steps that it has been alive is higher than T_{branch} (minimum tip development time that has to occur before the cell can branch), (2) that there are available surrounding positions to place a new branch cell, and (3) that the concentration of endothelial cells $n(i, j)$ is more considerable significant than $k_{\text{branch}}/c(i, j)$, where k_{branch} is a parameter that modulates the amount of branching that occurs for a given TAF concentration value. This final condition implies that cells will experience more frequent branching in regions near the tumor, with higher concentrations of Tumor Angiogenesis Factors (TAFs). When all prior conditions are met, the tip cell will be able to branch with a probability $c(i, j)/M_c$, where M_c is the maximum value for c over all the automaton cells.

Tests conducted with the model suggested that using the blood vessel grid values b in Eq. (13) resulted in a smoother propagation of tip cells. Thus, a proposed modification for such an equation that was found to be helpful in computational implementations of the model is the following:

$$n(i,j)^{\text{next}} = b(i,j) + P_{\text{center}}b(i,j) + P_{\text{left}}b(i,j-1) + P_{\text{right}}b(i,j+1) + P_{\text{up}}b(i-1,j) + P_{\text{down}}b(i+1,j) \quad (25)$$

Fig. 4 shows a blood vessel network evolved with the methods presented in this section. In the image, positions occupied by cancer cells in grid p of the tumor growth automaton have been indicated in green, while positions filled with blood vessels in matrix b of the angiogenesis model have been marked in red.

Once blood vessels reach the tumor, the system can be further evolved to simulate the behavior of proliferating cells within the continuously evolving vascular structure. Fig. 5 shows the vascular-supported growth of a tumor, evolved with a capillary network for 200 steps.

3.2. Graph representation of the blood vessel automaton

The angiogenesis cellular automata uses a matrix of blood vessels b, which indicates positions where vasculature is present. Conversion of this grid into a network with a set of vertices V and a set of edges E using the proposed algorithm summarized in Fig. 6.

As a preprocessing step, the binary image b is skeletonized, thinning it until a 1-pixel-wide representation of capillary branches is obtained.

Once the branches have been thinned, the recognition of pixels included as vertices of the graph can be performed. Two types of nodes are added to the vertices set V: branching points, which are positions surrounded by either 3 or 4 neighbor blood vessels in b, and terminal nodes, which are locations that have only one adjacent blood vessel neighbor. It is important to note that in this case, neighborhoods are composed only of the four cells (left, right, above, below) around the location in consideration.

On the other hand, recognition of edges proceeds by considering the grid location (i, j) of each identified vertex and searching for nearby vertices in blood vessel paths that start from such position. The exploration of paths can be conducted using a breadth-first-search algorithm (BFS), creating edges between found vertices and the one at (i, j). With BFS, the exploration is carried out within a Von-Neumann diamond-shaped neighborhood that progressively increases its radius, such as the one schematized in Fig. 6. The search was restricted to a predetermined number of iterations denoted as N_{BFS}. This approach was employed to manage the algorithm's computational time and confine the radius of vertices' influence, ensuring that vertices would only be connected to their closest nodes.

In addition to recognizing vertices and edges within b, we also examine associations between blood vessels and proliferating cells, designated as 1 in a matrix p. To accomplish this, we initiate the process by establishing a unique node to represent the tumor. Subsequently, an edge between a vertex and the tumor is established whenever a proliferating cell is detected in the 4-neighborhood of the respective node.

Fig. 7 shows the network representation of the blood vessel automaton image presented in Fig. 4. Here, the tumor node is denoted by a green central point, while nodes identified in b have been indicated with blue dots.

3.3. Effect of blood vessel's network metrics on tumor growth and radiotherapy

Conversion of the blood vessel grid into a network allowed us to examine how the properties of capillary system graphs were related to vascularized tumor growth and the outcome of simulated radiotherapy.

To conduct such tests, we first allowed a pre-evolved avascular tumor to develop in its angiogenic phase for 100 different values of the η parameter appearing in Eq. (17) (values ranged from 0 to 0.035). We generate 100 vascularized tumors, each with its distinct network features. The use of the eta parameter was based on previous testing, where we observed that variations of this quantity resulted in networks of different degree centralities. The total duration of this initial angiogenic growth was 200 steps.

Then, for all 100 innervated tumors, we performed point measurements of the following four network properties: (1) average degree centrality, (2) average betweenness centrality, (3) average page rank, and (4) average clustering coefficient.

Once the properties of each network had been determined, we allowed all tumors to develop further in 200 steps. We used the maximum Shannon's entropy computed in simulated tumor images across all 200 steps to assess tumor growth. As mentioned in Section 2.3, enlarged and dispersed tumors tend to present higher entropy values. J.A. Betancourt-Mar et al. conducted a thermodynamic study of tumor growth in [37], suggesting that the entropy production rate could be used to assess the metastatic potential of tumors. Conversely, Pedro Francisco Ferraz de Arruda et al. studied Shannon's entropy in prostate histological slides, finding that its value increases as the tissue develops hyperplasia and then cancer [38]. Based on such relation, vascular configurations that achieve maximum values for tumor entropy correspond to those that better support the dissemination of cancer cells.

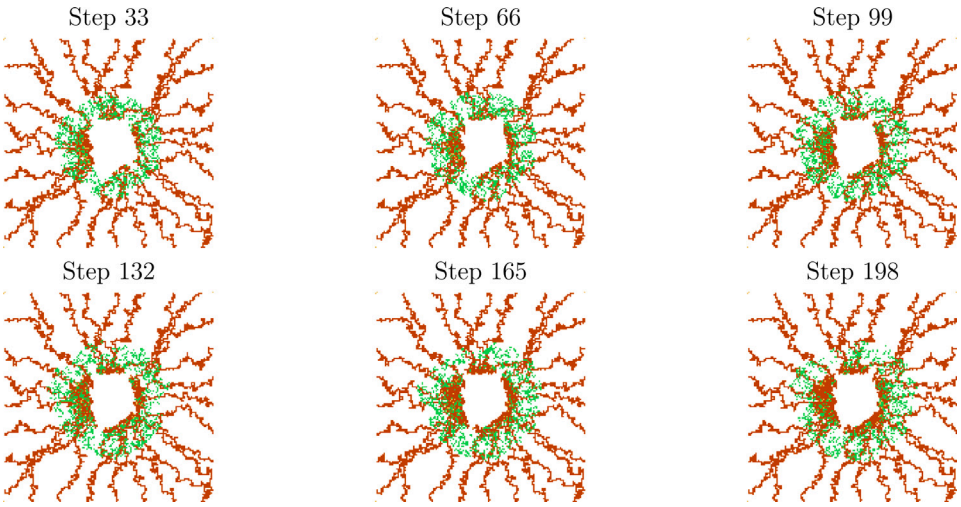

Fig. 5. Example of post-angiogenesis tumor growth. For this test, the tumor evolved for 300 steps, and blood vessel positions were used to determine locations where nutrients remained constant.

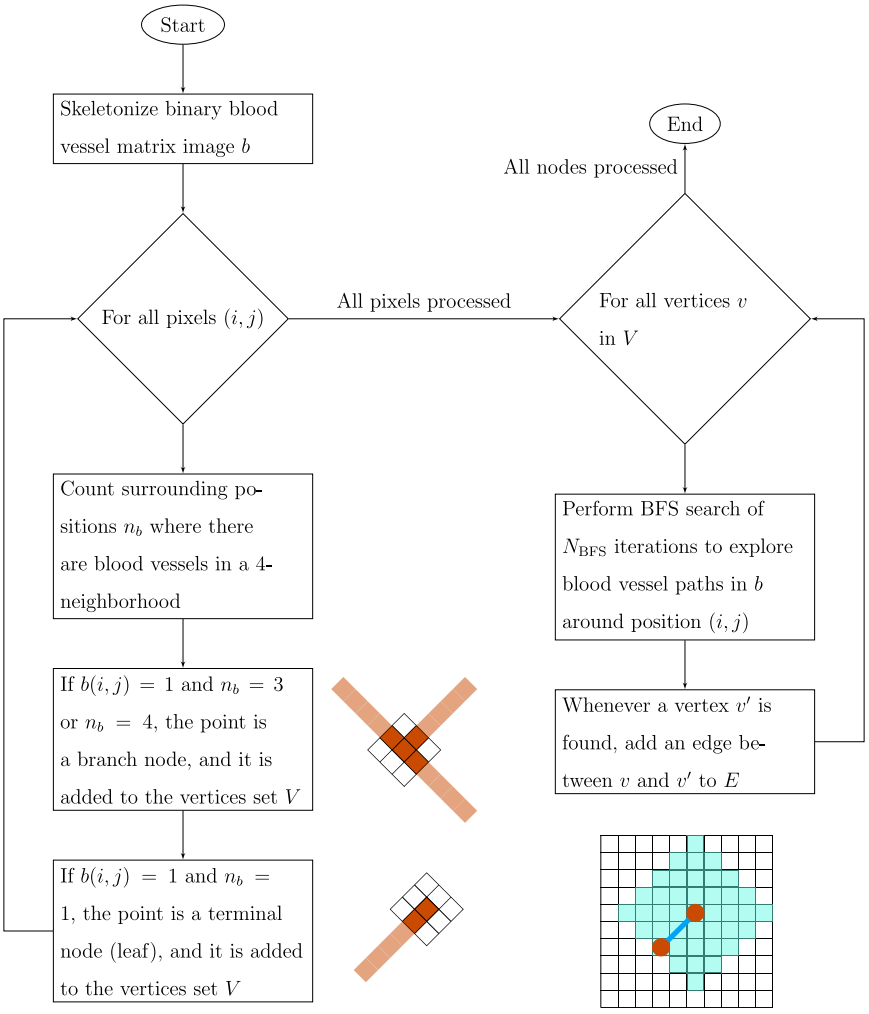

Fig. 6. Algorithm applied to transform the blood vessel automaton's grid into its network representation.

Fig. 8 compares initially registered network metrics and maximum entropy values reached by the tumor.

Analogous tests were conducted for a case where a radiotherapy treatment was administered to the developing tumor. In this case, however, the effectiveness of the treatment was assessed by computing the minimum entropy in the generated sequence of tumor images. Therapies applied to the tumor decrease entropy; thus, a lower minimum in entropy will be observed in cases where the treatment is most effective.

Fig. 9 shows how initial network metrics relate to the minimum tumor entropy value reached when applying the radiotherapy treatment.

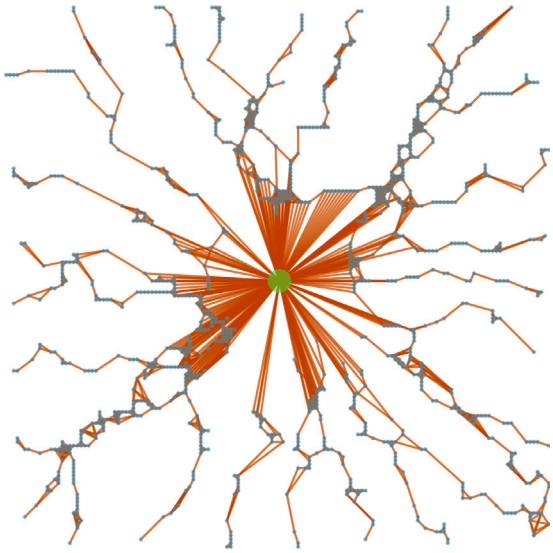

Fig. 7. Network representation of the evolved angiogenesis automaton presented in Fig. 4. A central green node represents the tumor and is connected to blood vessel nodes near proliferating cancer cells. The number of iterations used to explore nodes in this test was $N_{\text{BFS}} = 200$. (For interpretation of the references to color in this figure legend, the reader is referred to the web version of this article.)

3.4. Focused VDA treatment model

To study how targeting specific vertices of a vascular network affects tumor growth, we proposed a VDA treatment model, which can be administered at specific tumor locations.

To initialize the therapy, a binary matrix n_{ang} indicating the location of blood vessels that will be treated is supplied. Defining the set of positions (i', j') where $n_{\text{ang}} = 1$ as $\mathcal{A}$, a therapy potential P_{ang} can be computed at every location of the automaton as follows:

$$P_{\text{ang}}(i,j) = \begin{cases} k_{\text{ang}} M_{\text{ang}} + \sum_{(i',j')\in\mathcal{A}} \frac{k_{\text{ang}}}{\|(i,j)-(i',j')\|} & n_{\text{ang}}(i,j) = 1 \\ \sum_{(i',j')\in\mathcal{A}} \frac{k_{\text{ang}}}{\|(i,j)-(i',j')\|} & \text{otherwise} \end{cases} \tag{26}$$

where k_{ang} is a constant value parameter and M_{ang} is an amplification constant, established in such a manner that positions to be treated are assigned the most significant potential values. Once obtained, values for P are divided by the maximum therapy potential across all cells so that they remain bounded between 0 and 1.

At the start of the treatment, all cells with a potential value higher than a threshold T_{ang} are tagged to die at some point by adding them to an array D. Then, at each subsequent simulation step, a fixed fraction f_{ang} of cells are randomly sampled without replacement from set D, and nutrient value at the position occupied by such cells is fixed to zero. Such a process simulates a progressive cell death of blood vessels, which clinically can be achieved through vascular disrupting agents.

Fig. 10 shows the minimum tumor growth entropy observed when targeting the nodes in a vascular network that present the ten higher and smaller values for (1) degree centrality, (2) betweenness centrality, (3) page rank, and (4) clustering coefficient. Cases where therapy was most effective are those that exhibit fewer entropy minima.

To illustrate the evolution of the tumor under VDA therapy, Figs. 11 and 12 show the progression of tumor growth for cases where the ten nodes with higher and smaller degree centralities are respectively attacked. Positions of the ten nodes attacked in each case are indicated with blue markers.

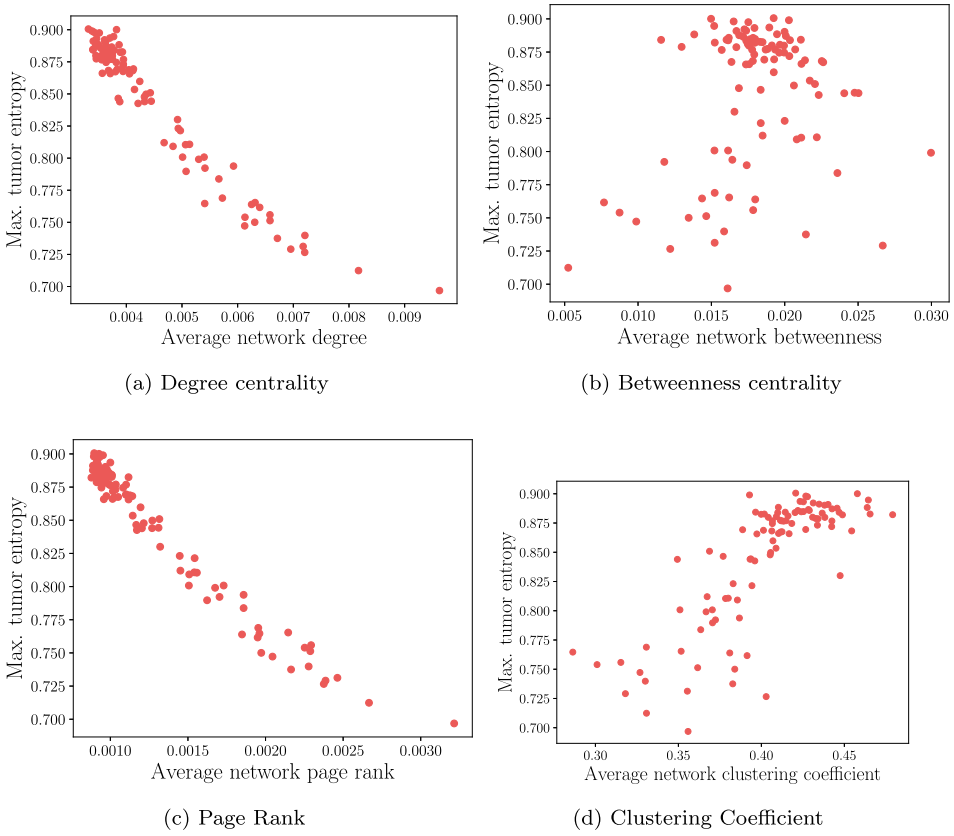

(a) Degree centrality (b) Betweenness centrality

(c) Page Rank (d) Clustering Coefficient

Fig. 8. Maximum entropy values obtained when simulating tumor growth with 100 different initial vascular networks (each point corresponds to a network). The horizontal axis represents an initial metric extracted from the network, where we examined (a) average degree centrality, (b) average betweenness centrality, (c) average page rank, and (d) average clustering coefficient. The vertical axis is the maximum entropy reached by the tumor (bigger values correspond to higher cell proliferation).

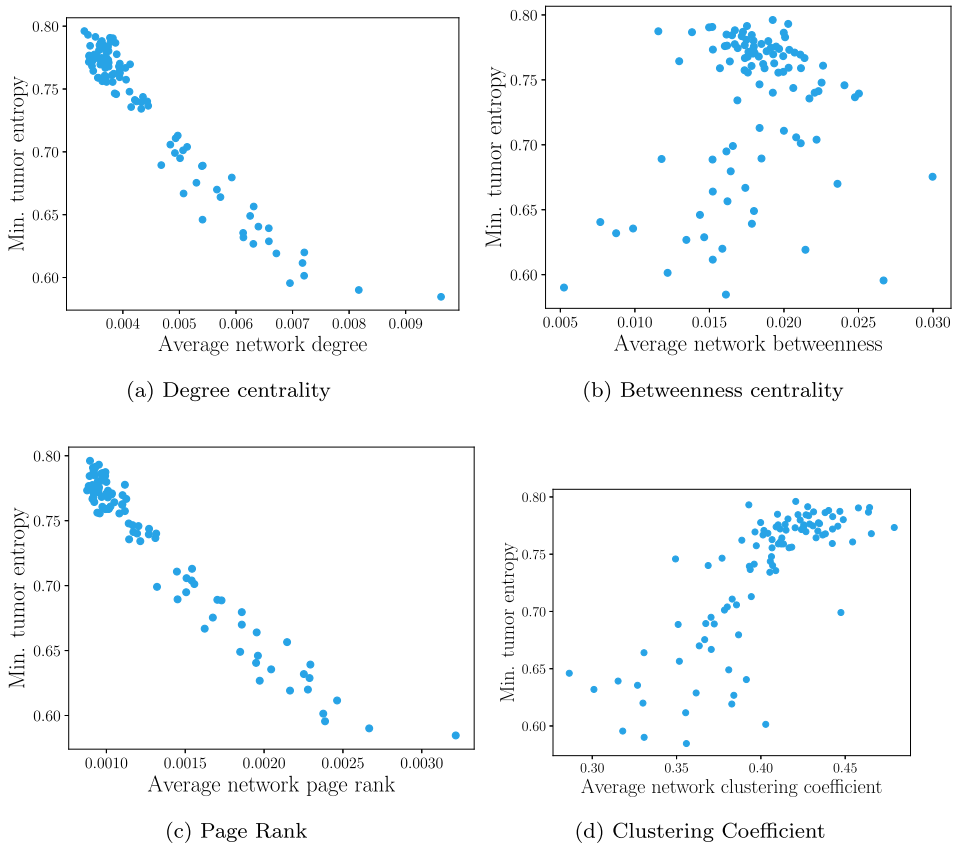

Fig. 9. Minimum entropy values reached when applying radiotherapy on a simulated tumor that has grown under the support of 100 different vascular network configurations (each point corresponds to one of the networks). The horizontal axis indicates a metric for the networks: (a) degree centrality, (b) betweenness centrality, (c) page rank, and (d) clustering coefficient. The vertical axis represents the minimum entropy obtained (smaller entropies correspond to better treatment outcomes). Radiotherapy parameter values used were $\gamma_{0,\mathrm{rad}} = 0.05$, $\alpha_{\mathrm{rad}} = 0.1$, $\beta_{\mathrm{rad}} = 0.05$, $d = 1$, $T_{n,\mathrm{rad}} = 0.35$, $P_{0,\mathrm{rad}} = 0.2$, $P_{f,\mathrm{rad}} = 0.5$.

4. Results and discussion

Fig. 5 shows how the simulated tumor evolves after a vascular network has been formed to supply it with nutrients. It can be observed that cancer cells expand outwards, favoring directions toward regions where blood vessels are densely packed. Thus, the model can mimic the faster-directed motility characteristic of the vascular phase [39].

Results for the relation between vascular network properties and tumor growth (Fig. 8) show that tumor growth is better supported with vascular networks that present on average high clustering coefficients and betweenness centralities, and low degree centralities and page ranks. An explanation of this result could be that vascular networks act as pathways for cancer cell migration. Thus, highly clustered nodes can provide the tumor with a clear path to follow, propelling its dissemination. Furthermore, having many in-between nodes can also be advantageous since they can redirect cells in new directions, providing flexible adaptive transit for cells. On the other hand, having too many nodes with a high degree of centrality can result in slow transportation of cancer cells because the multitude of connections for nodes can induce cyclic and random movement patterns within the network. It is known that scale-free networks such as the Internet facilitate information traffic, and these types of networks tend to present few nodes with high degree centralities [40]. Finally, high page-rank nodes can create stops for proliferating cells since many high transit paths are directed to them. Thus, a high average page rank could prevent the efficient spreading of tumor cells.

Fig. 9 illustrates the comparison between vascular network properties and the minimum tumor entropy values achieved upon application of radiotherapy treatment. The results indicate that higher treatment effectiveness is observed when the therapy is administered to tumors growing along with networks that offer less support to tumor growth. Specifically, these are networks with elevated average degree centralities, page ranks, and diminished average clustering coefficients and betweenness centralities. Consequently, the model's radiotherapy application can strategically exploit vulnerabilities in the blood vessel network's structure. As such, combining radiotherapy with treatments designed to disrupt the integrity of blood vessels around tumors could offer significant advantages. Certain studies have indicated promising outcomes through combinations of radiotherapy and VDA treatments, as radiotherapy effectively regulates the tumor micro-environment alterations induced by introducing vascular disrupting agents [41]. Nevertheless, it is essential to acknowledge that the interaction between these two treatments may entail potential risks related to radiation toxicity.

Results obtained with the proposed focused VDA therapy model (Fig. 10) showed that targeting nodes that provide local enhanced support to cell migration could be advantageous. Namely, we observed that targeting nodes with low centrality, low page rank, and high in-betweenness can improve therapy outcomes. These traits were identified as solid network features in our tumor growth and radiotherapy results. Interestingly, we found that focusing on nodes of low clustering that provide lesser support for migration was more advantageous for the clustering coefficient. Thus, like radiotherapy, VDA can exacerbate some pre-existing vulnerabilities in the network.

Finally, post-angiogenesis tumor evolution when vascular nodes with the higher and lower degree centralities are focused with VDA treatment have been shown respectively in Figs. 11 and 12. We note that attacking nodes that provide better tumor stability (those with low degree centrality) result in a quick breakage of the blood vessel network structure, disrupting nutrient supply to the tumor and inducing the death of a more significant number of proliferating cells.

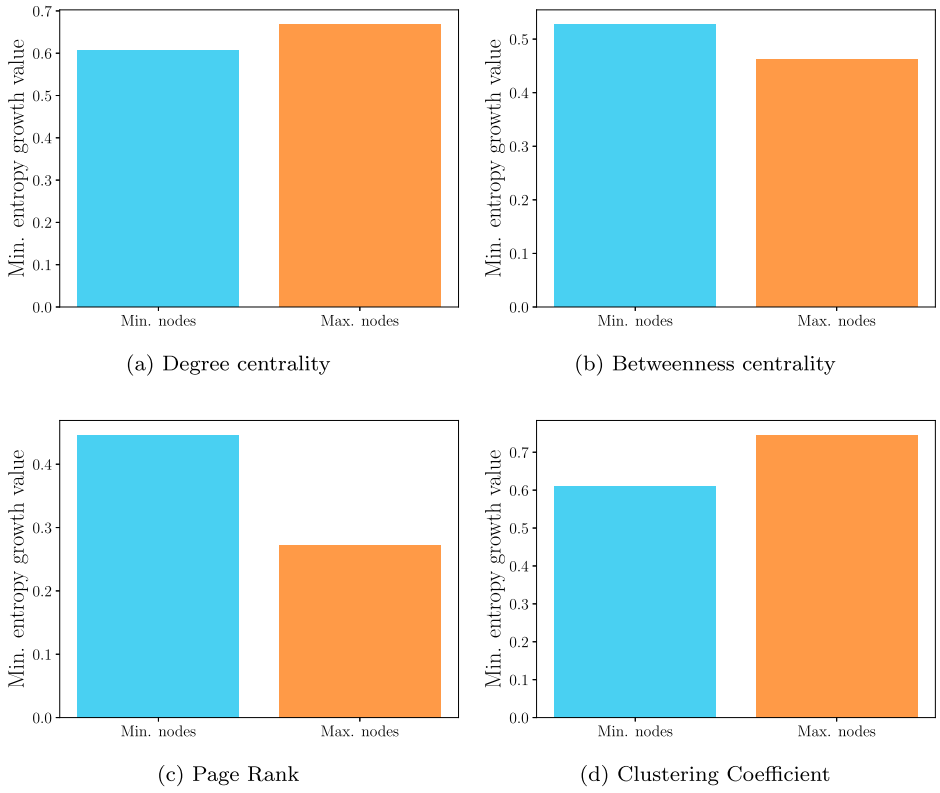

Fig. 10. Minimum tumor image entropy value obtained when applying VDA treatment to blood vessel nodes presenting the ten minimum and maximum values for (a) degree centrality, (b) betweenness centrality, (c) page rank, and (d) clustering coefficient. Lower entropy minima correspond to a more effective treatment. VDA parameters used in tests of this work were $k_{\text{ang}} = 1$, $M_{\text{ang}} = 2$, $T_{\text{ang}} = 0.04$, $f_{ang} = 0.1$.

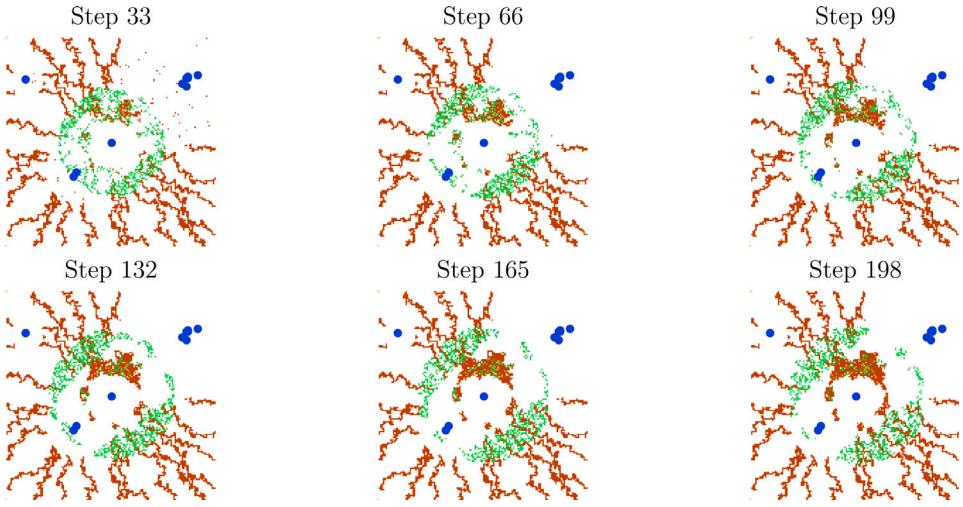

Fig. 11. Example of tumor evolution observed when applying the modeled VDA therapy. In this case, the treatment focused on areas near the ten vertices, which presented the highest degree of centrality values. Locations of the targeted nodes have been indicated with blue markers in all simulated images. (For interpretation of the references to color in this figure legend, the reader is referred to the web version of this article.)

Generally, results obtained with the VDA therapy model suggest that eliminating crucial supporting nodes in a vascular network can lead to essential stability breaks, hindering tumor development capabilities.

5. Concluding remarks

Our study illuminates the complex interplay between vascular networks and tumor growth, providing insights into potential therapeutic strategies. By employing cellular automata modeling, we have demonstrated the impact of vascular network properties on tumor behavior and response to therapy. Our findings highlight the importance of considering vascular structure and function in the design of cancer treatments.

Our model exhibits some qualitative traits observed during the angiogenic phase of cancer. Namely, it was found that vascular network nutrient supply results in an increase in proliferating cell motility. We propose a method for automaton-to-graph conversion that allows us to analyze vascular network properties and demonstrate the impact of point measurements of clustering coefficient, betweenness centrality,

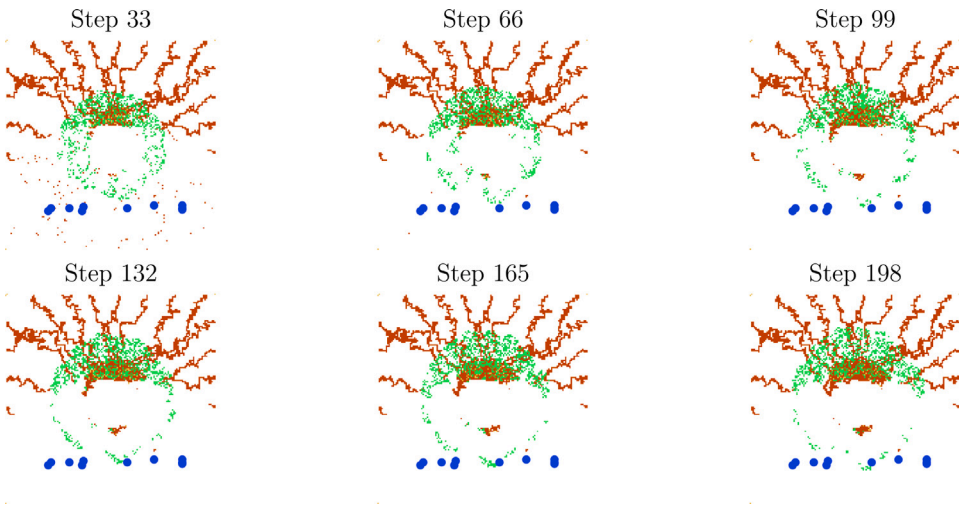

Fig. 12. Sample tumor evolution sequence obtained when applying the modeled VDA therapy. The treatment focused on areas close to the ten vertices presenting smaller degree centrality values for this simulation. Locations of the targeted nodes have been indicated with blue markers in all images. (For interpretation of the references to color in this figure legend, the reader is referred to the web version of this article.)

and node-specific metrics on tumor growth and some therapy modalities outcomes. At this theoretical stage, our findings are centered around qualitative observations. Calibrating the model to real-time scales and interaction strengths would necessitate experimental work beyond this study's scope.

Network analysis performed on the modeled blood vessel structure revealed distinct patterns: high clustering coefficient averages and betweenness centrality were found to increase tumor growth. In contrast, high average degree centrality and page rank can indicate less aggressive cancer variants.

Regarding the tested treatment modalities, simulated radiotherapy was observed to have a more significant impact on vascular networks, offering inadequate support for tumor growth. This observation underscores radiotherapy's potential to exploit vulnerabilities in the blood vessel structure.

Our proposed model for VDA therapy achieved better control over cancer development when targeting nodes possessing network metric values identified as enhancers of tumor growth. These strategic targets, pivotal in fortifying the vascular network, demonstrated the potential for rapid disruptions in the global structure of the network, hindering the dissemination of proliferating cancer cells. Furthermore, the synergistic combination of radiotherapy with anti-angiogenic therapy, specifically Vascular Disrupting Agents (VDAs), presents a promising avenue, aligning with proposals from prior studies. It is worth noting that the practical implementation of such combined approaches mandates meticulous protocols to mitigate radiation toxicity, a critical consideration in clinical contexts.

This work focused on the simulation and analysis of synthetic data, presenting an alternative model that can be used to study cancer growth in its vascular phase, featuring novel tools for analyzing how network structure affects tumor development and treatment. A posterior phase in our research would bridge this gap by applying similar techniques to real-world instances, verifying how network properties affect prognosis in distinct tumor types and stages. Additionally, our ongoing work includes incorporating more complex biological factors and validating them with clinical data. By exploring the dynamic nature of vascular networks across diverse tumor types and stages, we aim to uncover nuanced patterns, guiding tailored treatment strategies. Furthermore, understanding the interplay between genetic mutations and vascular properties might offer deeper insights into personalized therapeutic interventions.

In summary, our study represents a significant step towards unraveling the complexities of post-angiogenic tumor growth and advancing personalized cancer therapy. Continued interdisciplinary efforts will be essential in translating these findings into clinical applications and ultimately improving patient outcomes.

Funding

The research leading to these results received funding from CONAHCYT-Mexico under Grant Agreement Fronteras 2019-217367.

CRediT authorship contribution statement

Juan Uriel Legaria-Peña: Writing – review & editing, Writing – original draft, Visualization, Validation, Software, Methodology, Investigation, Formal analysis. **Félix Sánchez-Morales:** Writing – review & editing, Writing – original draft, Visualization, Validation, Software, Methodology, Investigation, Formal analysis. **Yuriria Cortés-Poza:** Writing – review & editing, Writing – original draft, Validation, Supervision, Project administration, Methodology, Investigation, Funding acquisition, Formal analysis, Conceptualization.

Declaration of competing interest

The authors of this research article declare that they have no conflicts of interest to disclose.

Data availability

No data was used for the research described in the article.

References

[1] Reyes-Aldasoro CC. The proportion of cancer-related entries in PubMed has increased considerably; is cancer truly "the emperor of all maladies"? PLoS One 2017;12.
[2] Grizzi F, Chiriva-Internati M. Cancer: looking for simplicity and finding complexity. Cancer Cell Int 2006;6(4).
[3] Gentles AJ, Gallahan D. Systems biology: Confronting the complexity of cancer. Cancer Res 2011;71.
[4] Folkman J. Role of angiogenesis in tumor growth and metastasis. Semin Oncol 2002;29:15–8.
[5] Fouladzadeh A, Dorraki M, Min KKM, Cockshell MP, Thompson EJ, Verjans JW, Allison A, Bonder CS, Abbott D. The development of tumour vascular networks. Commun Biol 2021;4(1111).
[6] Chimal-Eguía JC, Castilo-Montiel E, Paez-Hernández RT. Properties of the vascular networks in malignant tumors. Entropy 2020;22.

[7] Topa P, Dzwinel W. Using network descriptors for comparison of vascular systems created by tumor-induced angiogenesis. Theor Appl Inform 2009;21(2).
[8] Stolz BJ, Kaeppler J, Markelc B, Braun F, Lipsmeier F, Muschel RJ, Byrne HM, Harrington HA. Multiscale topology characterizes dynamic tumor vascular networks. Sci Adv 2022;8(23).
[9] McDougall SR, Anderson AR, Chaplain MA. Mathematical modelling of dynamic adaptive tumour-induced angiogenesis: Clinical implications and therapeutic tarteging strategies. J Theoret Biol 2006;241:564–89.
[10] Sadhukhan S, Mishra P. The notion of fractals in tumour angiogenic sprout initiation model based on cellular automata. Chaos Solitons Fractals 2022;155.
[11] Plank MJ, Sleeman BD. A reinforced random walk model of tumour angiogenesis and anti-angiogenic strategies. Math Med Biol: J IMA 2003;20.
[12] Shirinifard A, Gens JS, Zaitlen BL, Popławski NJ, Swat M, Glazier JA. 3D multi-cell simulation of tumor growth and angiogenesis. PLoS One 2009;4(10):e7190.
[13] Legaria-Peña JU, Sánchez-Morales F, Cortés-Poza Y. Evaluation of entropy and fractal dimension as biomarkers for tumor growth and treatment response using cellular automata. J Theoret Biol 2023;564.
[14] Griffioen AW. Angiogenesis. In: Encyclopedia of cancer. Springer; 2017, p. 185–6.
[15] Ellis L, Fidler I. Angiogenesis and metastasis. Eur J Cancer 1996;32.
[16] Hillen F, Griffioen AW. Tumor vascularization: sprouting angiogenesis and beyond. Cancer Metastasis Rev 2007;26:489–502.
[17] Alberts B, Johnson A, Lewis J, Morgan D, Raff M, Roberts K, Walter P. Molecular biology of the cell. 6th ed.. Taylor & Francis; 2015, p. 1237–9, ch. 23.
[18] Zakirov B, Charalambous G, Thuret R, Aspalter IM, Van-Vuuren K, Mead T, Harrington K, Regan ER, Herbert SP, Bentley K. Active perception during angiogenesis: filopodia speed up notch selection of tip cells in silico and in vivo. Philos Trans R Soc B 2021.
[19] Chen W, Xia P, Wang H, Tu J, Liang X, Zhang X. The endothelial tip-stalk cell selection and shuffling during angiogenesis. J Cell Commun Signal 2019;13:291–301.
[20] Efthymiou G, Saint A, Ruff M, Rekad Z, Ciais D, Obberghen-Schilling EV. Shaping up the tumor microenvironment with cellular fibronectin. Front Oncol 2020;10.
[21] Stenzel D, Lundkvist A, Sauvaget D, Busse M, Graupera M, van der Flier A, Wijelath ES, Murray J, Sobel M, Costell M, Takahashi S, Fässler R, Yamaguchi Y, Gutmann DH, Hynes RO, Gerhardt H. Integrin-dependent and -independent functions of astrocytic fibronectin in retinal angiogenesis. Development 2011;138.
[22] Jaffe EA, Mosher DF. Synthesis of fibronectin by cultured human endothelial cells. J Exp Med 1978;147.
[23] Gatenby RA, Silva AS, Gillies RJ, Frieden BR. Adaptive therapy. Cancer Res 2009;69:4894–903.
[24] Boulefour W, Rowinski E, Louati S, Sotton S, Wozny A-S, Moreno-Acosta P, Mery B, Rodriguez-Lafrasse C, Magne N. A review of the role of hypoxia in radioresistance in cancer therapy. Med Sci Monit 2021.
[25] Serensen BS, Horsman MR. Tumor hypoxia: Impact on radiation therapy and molecular pathways. Front Oncol 2020;10.
[26] Marmé D. Tumor angiogenesis: A key target for cancer therapy. Oncol Treat Res 2018;41.
[27] Smolarczyk R, Czapla J, Jarosz-Biej M, Czerwinski K, Cichoń T. Vascular disrupting agents in cancer therapy. Eur J Pharmacol 2021;891.
[28] Lefever R, Erneaux T. On the growth of cellular tissues under constant and fluctuating environmental conditions. In: Nonlinear electrodynamics in biological systems. Springer; 1984, p. 287–305.
[29] Shahmoradi S, Rahatabad FN, Maghooli K. A stochastic cellular automata model of growth of avascular tumor with immune response and immunotherapy. Inform Med Unlocked 2018;12:81–7.
[30] Brüningk SC, Ziegenhein P, Rivens I, Oelfke U, ter Haar G. A cellular automaton model for spheroid response to radiation and hyper thermia treatments. Sci Rep 2019;9(17674).
[31] Fowler JF. The linear-quadratic formula and progres in fractionated radiotherapy. Br J Radiol 2024;62(740).
[32] McMahon SJ. The linear quadratic model: usage, interpretation and challenges. Phys Med Biol 2018;64(1).
[33] Ferreira JAG, Olasolo JJ, Azinovic I, Jeremic B. Effect of radiotherapy delay in overall treatment time on local control and survival in head and neck cancer: Review of the literature. Rep Pract Oncol Radiother 2015;20.
[34] Anderson A, Chaplain M. Continuous and discrete mathematical models of tumor-induced angiogenesis. Bull Math Biol 1998;60.
[35] Peña L, Sanchez-Morales, Cortes-Poza. Angiogenesis model. 2024, https://github.com/walup/Synchro_Angiogenesis_Model/tree/main. [21 April 2024].
[36] Chaplain M. The mathematical modelling of tumour angiogenesis and invasion. Acta Biotheor 1995;387–402.
[37] Betancourt-Mar J, Llanos-Pérez J, Cacho G, mansilla R, Martin R, Montero S, Villar JN. Phase transitions in tumor growth: IV relationship between metabolic rate and fractal dimension of human tumor cells. Phys A 2017;473:344–51.
[38] de Arruda PFF, Gatti M, Nestor F, Junior F, de Arruda JGF, Moreira RD, Junior LOM, de Arruda LF, de Godov MF. Quantification of fractal dimension and Shannon's entropy in histological diagnosis of prostate cancer. BMC Clin Pathol 2013;13(6).
[39] Zetter BR. Cell motility in angiogenesis and tumor metastasis. Cancer Invest 1990;8:669–71.
[40] Pastor-Satorras R, Vespiagnani A. Epidemic spreading in scale-free networks. Phys Rev Lett 2001;86.
[41] Ciric E, Sersa G. Radiotherapy in combination with vascular-targeted therapies. Radiol Oncol 2010;44.